Fluid–structure interaction between a pendulum and monochromatic waves

Bos, R. W.; Wellens, P. R.

DOI
10.1016/j.jfluidstructs.2020.103191

Publication date
2021

Document Version
Final published version

Published in
Journal of Fluids and Structures

Journal of Fluids and Structures 100 (2021) 103191

Contents lists available at ScienceDirect

Journal of Fluids and Structures

journal homepage: www.elsevier.com/locate/jfs

Fluid–structure interaction between a pendulum and monochromatic waves

R.W. Bos, P.R. Wellens *

Technische Universiteit Delft, Mekelweg 2, 2628 CD, Delft, Netherlands

ARTICLE INFO

Article history:
Received 19 May 2020
Received in revised form 5 November 2020
Accepted 12 November 2020
Available online 2 December 2020

ABSTRACT

Maritime structures operating out at sea experience large changes in wetted area because of free surface waves. Although these conditions are typical for maritime applications, a fundamental experiment that includes a structure in the air–water interface undergoing transitions from dry to wet and back does not appear to exist. This paper aims to fill that knowledge gap. We present an experiment in which a pendulum is suspended just above the still water level and then exposed to monochromatic free surface waves with different wave lengths. Additionally a reduced-order model is derived to compute the response of the pendulum and help interpret the experimental results.

The motion response of the pendulum is demonstrated to depend highly on whether the wave period is much lower or higher than the dry natural period of the pendulum. Additionally, a sensitivity study with the wave amplitude in the model and a quantification of the variability in the experiment both indicate that the variability in the motion response of the pendulum is increased with respect to the variability of the incoming wave. We believe this experiment and the results make for an interesting benchmark of fluid–structure interaction in free surface waves. The properties of the pendulum and the experiment are available as open data at doi:10.4121/13187594 (Wellens and Bos, 2020).

1. Introduction

Ships and offshore structures are subject to waves, and being able to predict how the structure responds is important for safety and efficiency. A ship operates in the interface between water and air and undergoes motion as a result of the interaction with free surface waves. This fluid–structure interaction (FSI) commonly is modelled assuming small waves and taking the wetted surface of the ship constant, such as in added resistance (Kim et al., 2017; Feng et al., 2017; Bennett et al., 2013). Also when assessing the hydroelasticity of ice sheets in the ocean (Porter, 2019) or a multi-body wave energy harvester (Zheng and Zhang, 2017), the wetted surface is considered constant. We are however interested in the situation in which interaction with waves causes large variations of the wetted surface of the structure. Typical examples of these situations are the speed loss of ships sailing through large waves and the speed variations of a planing ship in initially calm water. Moreover the large change in wetted area and the interaction between the load and the structure has potentially a large effect on the load, as is described for sloshing model tests in Lugni et al. (2014). Existing models to describe these effects are limited, and therefore numerical methods such as Computational Fluid Dynamics (CFD) need to be used to evaluate them.

* Corresponding author.
E-mail addresses: r.w.bos@tudelft.nl (R.W. Bos), p.r.wellens@tudelft.nl (P.R. Wellens).

https://doi.org/10.1016/j.jfluidstructs.2020.103191

We focus on the interaction of water waves with maritime structures, which is characterized by the following three points:

1. The average density of the structure is approximately equal to the average density of the fluid (required for buoyancy, and in contrast to for instance an airplane, which is held in air by lift). Because of this, maritime structures generally have a large added mass. This is important because a small change in wetted area could give a large change in added mass.
2. The change in wetted area is large and varies constantly due to water waves and structure motion
3. The motion of the structure is large, oscillatory and originates primarily from the rigid body modes. The structure is increasingly stiff going to more local vibration modes

It is a challenge is to find validation cases for FSI codes which satisfy all aforementioned points. For instance Weidenfeld and Arad (2018), require FSI to consider the sound of a flapping airfoil, Sader et al. (2016) study large-amplitude, vortex-induced vibration of an inverted flag. These are typical examples of FSI, but they do not satisfy our criteria 1 and 2. One validation experiment describes a sloshing tank with a continuously submerged beam that deforms in waves as the tank is rotated (Botia-Vera et al., 2010); this study does not satisfy criterion 2. Another experiment is a dam break held back by an elastic flap (Liao et al., 2015) or a dam break on a vertical cylinder (Kamra et al., 2019). In the latter two, the structure transitions from wet to dry (criterion 2), but does not undergo the back-and-forth motion induced by free surface waves (criterion 3). Losada and Merino (1987) study incipient motion of sea bed particles in waves. Draycott et al. (2019) consider wave loading on horizontal axis tidal turbines. The experiment of Castellino et al. (2018) includes the variations of the wetted surface of a fixed wall with a parapet. Young et al. (2020) investigates the hydroelastic response of a vertical strut in waves, while Hayatdavoodi and Ertekin (2015) and Hayatdavoodi et al. (2019) deal with submerged plates and decks in waves. These references feature motion, sometimes large (criterion 3), but they do not account for large variations in wetted area (criterion 2). Summarizing, to our knowledge there are no existing benchmark problems that satisfy all our demands at the same time.

In order to fill this gap, we propose a fundamental benchmark problem to validate numerical codes for maritime FSI applications. The novelty with respect to existing literature is that we study a structure in the interface between water and air that undergoes motion as its surface changes from dry to wet in non-breaking waves. As a model for the structure we choose a pendulum. Earlier Mathai et al. (2019) studied the free decay of a pendulum that is always submerged, Andreeva et al. (2016) studied the dynamics of a pendulum loaded by analytical models of wave profiles, Lenci et al. (2012) and Lenci and Rega (2011) studied a pendulum on a barge that is excited by waves. Ours is suspended above the mean free surface and then periodically loaded by monochromatic waves. Therefore this experiment satisfies all three criteria. With our experiment, we answer the following question: *How does an initially dry structure respond to monochromatic wave loading?* In other words, our objective is to use the pendulum to obtain a more fundamental understanding of the interaction of a maritime structure with free surface waves.

The experimental data and a description thereof are available as open data (Wellens and Bos, 2020).

2. Experiment

The experiment was conducted in the small towing tank of Delft University of Technology. A schematic overview of the pendulum above the towing tank is shown in Fig. 1. It shows the pendulum together with three wave gauges. The left side of the overview shows the wave dissipating beach, the right side shows the wave maker. The axis system of the experiment is at the horizontal position of the wave maker at the vertical position of the mean free surface. We have chosen the positive x axis in the propagation direction of the waves, and the angle of the pendulum is positive when it moves along with the waves.

Fig. 2 shows photos of the front and side view of the experimental setup. The front view shows the pendulum suspended from the towing carriage. It also shows that extra care was taken to rigidly fix the frame supporting the bearings by shoring it to the carriage with transverse braces. The right image shows the pendulum from the side of the tank with the wave gauge nearest to the pendulum in the background.

The pendulum consists of two parts: the frame and the tube. The frame is made of aluminium profiles and connected with two bearings to the towing carriage. Thin strips, which are assumed to be drag free, connect the frame to the tube. In this way only the tube experiences hydrodynamic loading and not the frame. The tube is positioned 10 mm above the mean free surface level, with the pendulum fulcrum at 1050 mm above the centre of the tube. A PVC tube with a diameter of 50 mm and a length of 1500 mm was chosen.

It is taken nearly as long as the tank is wide to make 3D wave interaction effects negligible compared to the overall loading, yielding essentially a 2D experiment. We chose a tube because the shape does not change when it rotates. The drag coefficient, therefore, does not depend on the angle of the pendulum. End caps are fitted to the tube to make it watertight.

The pendulum is positioned 29.880 m away from the wave maker. The wave maker rotation is prescribed and the generated waves pass three wave gauges: one in front of the pendulum, one at and one behind it. Measured with a laser distance metre, they are at 25.849 m, 29.880 m and 34.666 m from the wave maker. When wave interaction with the tube begins, the pendulum starts rotating, which is measured by a potentiometer. The pendulum was weighed on a scale to a

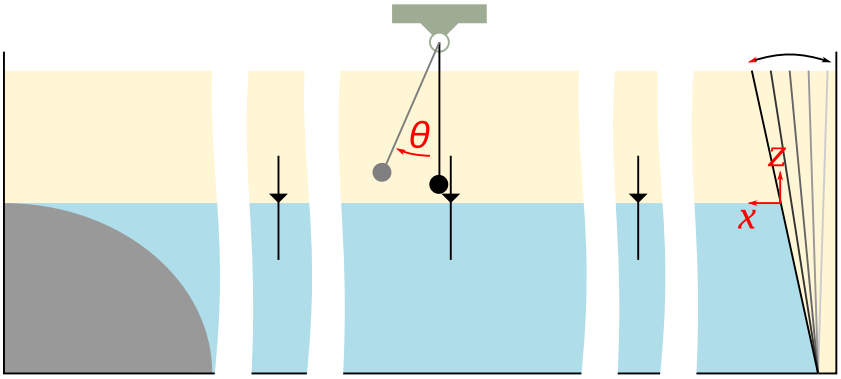

Fig. 1. Schematic overview of the experimental setup. At the far left side the beach, at the far right the wave maker with the axis system. In between, the three wave gauges at 25.849 m, 29.880 m and 34.666 m from the wave maker, as well as the pendulum at 29.880 m from the wave maker.

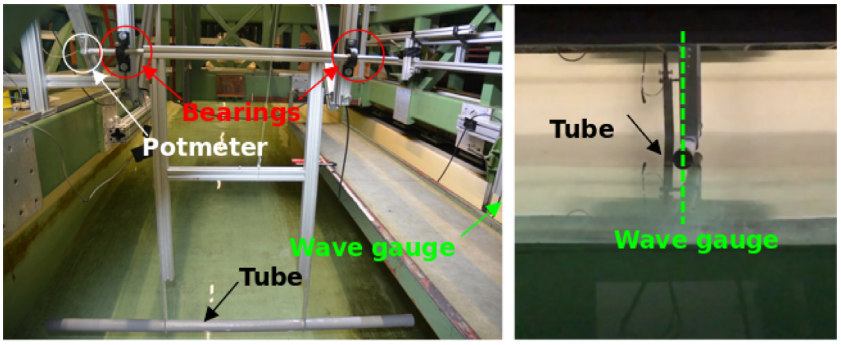

Fig. 2. Photos from front (left) and side (right) of the experimental setup, showing the frame, bearings, potentiometer and wave gauge nearest to the pendulum. These photos are a close-up of Fig. 1.

Table 1
Name, position and error of the three wave gauges in the experiment.

Name	Position	To Pendulum	Measurement error
WHM 1	Side of the wave maker	−4.031 m	0.5 mm
WHM 2	At pendulum	0.000 m	0.3 mm
WHM 3	Side of the beach	4.786 m	0.6 mm

mass of 8.86 kg. The centre of gravity was found by putting it over a support and moving it until stable. It was positioned at 365 mm from the fulcrum, giving a restoring force coefficient $k = 31.7$ N m rad^{-1}.

The potentiometer is calibrated by giving it 10° rotations within its measuring range and fitting a straight line. Over the complete range the maximum error with respect to the fitted calibration factor is within 0.5°. The wave gauges are calibrated by measuring the output at 20 mm intervals and also fitting a straight line. Table 1 shows the names, positions with respect to the pendulum and maximum errors with respect to the calibration of the wave gauges.

At the beginning of each test the average signal of the first second defines the new 'zero', for which the entire signal is corrected; this corrects for drift in the wave gauges. All measurements are taken at 1000 Hz and then passed through a 100 Hz analog second order low pass filter. Additionally, we applied a digital moving average filter with a width of 25 samples for four times to remove higher vibration modes of the pendulum.

The wave maker generates waves according to a sine wave modulated with a window function to slowly ramp up the signal towards the desired amplitude and then down again. The signal is held at the desired amplitude for 50 s.

Each test features one wave length: $\lambda = 1$, 3, 5 or 7 m, with three repetitions for each wave length to get a quantification of the variability between experiments. The water depth was kept at 994 mm for all experiments, a wave amplitude of 50 mm was desired. Two measures were taken to keep the starting conditions for each experiment the same. First, because shorter wave modes dissipate faster, the tests were done in a series of increasing wave length. Second, a waiting time of 15 min was taken between tests to allow the water in the tank to come to rest. The effectiveness of these measures is assessed in the results section.

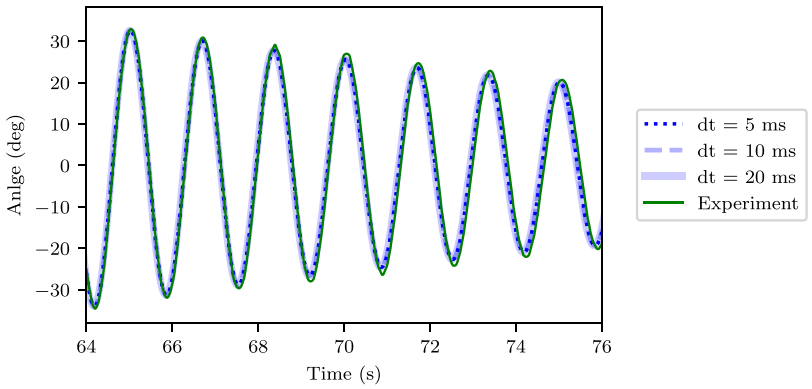

Fig. 3. Reduced-order model of free pendulum decay fitted to the experiment, with convergence study for the time step.

3. Analytical model

To better understand the experimental results we will use an analytical model based on the following assumptions. The pendulum has only one degree of freedom: rotation about its fulcrum. Only the tube at the bottom of the pendulum experiences a hydrodynamic force, which is constant along the length of the tube (width of the towing tank). Every occurrence of wave interaction in our experiment has four phases:

1. Water entry: the wetted area increases over time (Wagner, 1932; Mei et al., 1999)
2. Submerged motion: fully wet, with mostly drag and buoyancy (Morison et al., 1950; Mathai et al., 2019)
3. Water exit: wetted area decreases over time
4. Free vibration: only air and friction damping (Dolfo et al., 2016)

Water entry and exit can generate high peak pressures (Van Nuffel et al., 2014; Mathai et al., 2015), which are generally localized in space and time. Because the pendulum integrates all local pressures in its global motion we will assume that we can neglect peak pressures. The buoyancy force acts upward and is multiplied with the position and sine of pendulum angle to obtain the moment on the pendulum. For small angles, the moment is small and therefore ignored. Other studies Dolfo et al. (2016) mention that the air drag is small, and therefore it is not taken into account here. We will reflect upon these assumptions in the results section.

The following reduced-order model describes how the pendulum responds after the interaction with the waves starts. The first component of the model is the equation of motion of the pendulum:

$$I\ddot{\theta} + c\dot{\theta} + k\sin\theta = M \tag{1}$$

where I is the inertia, c damping and k the restoring force coefficient, with θ the instantaneous angular position and M an external moment. We performed a free vibration test with the pendulum to determine these parameters. By taking the first and second time derivative of the angle we obtain the angular velocity and acceleration. These are substituted into the equations of motion to find the inertia and damping with a least squares approximation. With $k = 31.7$ N m rad^{-1} found as described above, we obtain the values $I = 2.17$ kg m^2 and $c = 0.205$ N m s rad^{-1}.

Fig. 3 shows the free vibration of the experiment and reduced-order model (with M in Eq. (1) equal to 0) for the same starting position. Eq. (1) was rewritten in a state-space representation and integrated numerically with two-stage Runge–Kutta. The figure shows results for three time steps: 20, 10 and 5 ms. Reducing the time step from 20 ms to 5 ms does not bring about a significant change in error: 0.2% comparing the final maxima. We however choose to use the 5 ms time step to have enough temporal resolution to capture the period of the shortest waves (period $T = 0.8$ s for $L = 1$ m) with more than 150 time steps. The reduced-order model in Fig. 3 shows a slightly faster decay than the experiment, which is likely because the actual dissipation mechanisms require more elaborate modelling than a linear damping coefficient. However, at the last shown maximum angle after 7 full periods of 1.64 s, the reduced-order model is only 0.07 s and 0.5° behind the experiment. This error is smaller than the calibration error of the potentiometer, and therefore acceptable. In comparing the model with the experiment, the time integration error has even less influence, because repeated wave forcing takes place in intervals of at most 2.5 s (period of the longest wave of 7 m), and the modelling error of the wave force is larger than the numerical error.

The forcing on the pendulum M is modelled as the cross product of moment arm, given as $L = 1050$ mm above, and the hydrodynamic force on the tube F_m scaled by a factor β:

$$M = \beta F_m L\cos\theta \tag{2}$$

The reason for scale factor β is elaborated upon below. The force on the tube per unit width is given by the Morison equation (Morison et al., 1950):

$$F_m = \rho \left(C_m V a + \frac{1}{2} C_d A |u| u \right) \tag{3}$$

Here, ρ is the density of water, taken as 1000 kg m^{-3}. Parameters C_d, C_m are the added mass and drag coefficients based on the Keulegan–Carpenter number KC, which can be found in Sarpkaya (1986). Variables a, u are the acceleration and velocity of the water relative to the pendulum. The frontal area and volume of the cylinder are given by A and V.

One of the key ingredients of our experiment is the large change in wetted area. Since the pendulum is not completely wet or dry all the time we need another function to estimate the wet surface. How the force on a horizontal member depends on the wet surface was hypothesized before by Kaplan and Silbert (1976), who alter drag and added mass coefficient with an analytical model, yet without validation. They describe only vertical forces, where we need a model for the horizontal force. In the model we approximate the varying wetness with a scaling factor for the Morison equation: our novel wetness parameter β. This parameter is 0 for a dry cylinder and 1 for a fully submerged cylinder, and linearly scales based on the submersion depth at the centre of the tube:

$$\beta = \max \left(\min \left(\frac{\eta - (z_p - D/2)}{D}, 1 \right), 0 \right) \tag{4}$$

where D is the tube diameter, η wave elevation and z_p the instantaneous vertical position of the centre of the tube. Note that for an underwater pendulum $\beta = 1$, which yields the equation of motion in Mathai et al. (2019). While this wetness function is a large simplification of the physics that take place with water entry and exit, we believe it can be seen as a suitable approximation to explain the results of the experiments.

In our model we first assume that the free surface waves satisfy small amplitude potential flow, or Airy theory. Disregarding start-up effects and reflection from the beach, the surface elevation is then described by:

$$\eta = \eta_a \cos(k_w x - \omega t)$$

where ω, k_w are the angular velocity and wave number, and η_a is the amplitude. The velocity and acceleration of a fluid particle in horizontal direction are:

$$u_p = \eta_a \omega \frac{\cosh(k(z+h))}{\sinh(kh)} \cos(k_w x - \omega t) \tag{5}$$

$$a_p = \eta_a \omega^2 \frac{\cosh(k(z+h))}{\sinh(kh)} \sin(k_w x - \omega t) \tag{6}$$

For the Morison equation we however need the relative velocity and acceleration of the water with respect to the pendulum:

$$u = L \cos\theta \dot{\theta} - u_p \tag{7}$$

$$a = L \cos\theta \ddot{\theta} - L \sin\theta \dot{\theta}^2 - a_p \tag{8}$$

Velocities and accelerations above the still water level are obtained by constant extrapolation from the value at the mean free surface position.

The interaction between waves and pendulum is a nonlinear process. For the chosen steepnesses the waves themselves are also nonlinear, albeit mildly. In order to investigate how important this wave nonlinearity is, the reduced order model was equipped with the nonlinear steady wave solution proposed by Rienecker and Fenton (1981). This is a wave solution that follows from fitting a truncated Fourier series to the nonlinear flow equations and nonlinear boundary conditions at the initially unknown instantaneous position of the free surface. The solution features no errors other than from truncating the Fourier series. As such, it is a more suitable approach for modelling the waves in our experiment in limited water depth, than the more often used nonlinear Stokes steady wave solution that is based on an expansion around the mean free surface with an expansion error and the requirement that the water depth should be sufficiently deep for the expansion to converge. Our nonlinear waves with the Rienecker–Fenton approach were solved with $N = 16$ Fourier components and converged until the error was smaller than 10^{-10}.

In order to determine the forces on the tube we need to use the drag and added mass coefficients C_d and C_m. These coefficients depend on the Keulegan–Carpenter number, in which we use the particle velocity, wave period and tube diameter. Since we use constant extrapolation for velocities above the water we substitute the amplitude at $z = 0$ m from Eq. (5):

$$KC = \frac{UT}{D} = \frac{\eta_a \omega \frac{\cosh(k(z+h))}{\sinh(kh)} \frac{2\pi}{\omega}}{D} = \frac{2\pi \eta_a}{D} \tag{9}$$

which, by using 50 mm for the diameter D of the tube and 50 mm for η_a, gives $KC \approx 6$. From Sarpkaya (1986) we find $C_d = 2.0$ and $C_m = 1.0$ for our setup. Note that two assumptions are made here. First, choosing the particle velocity

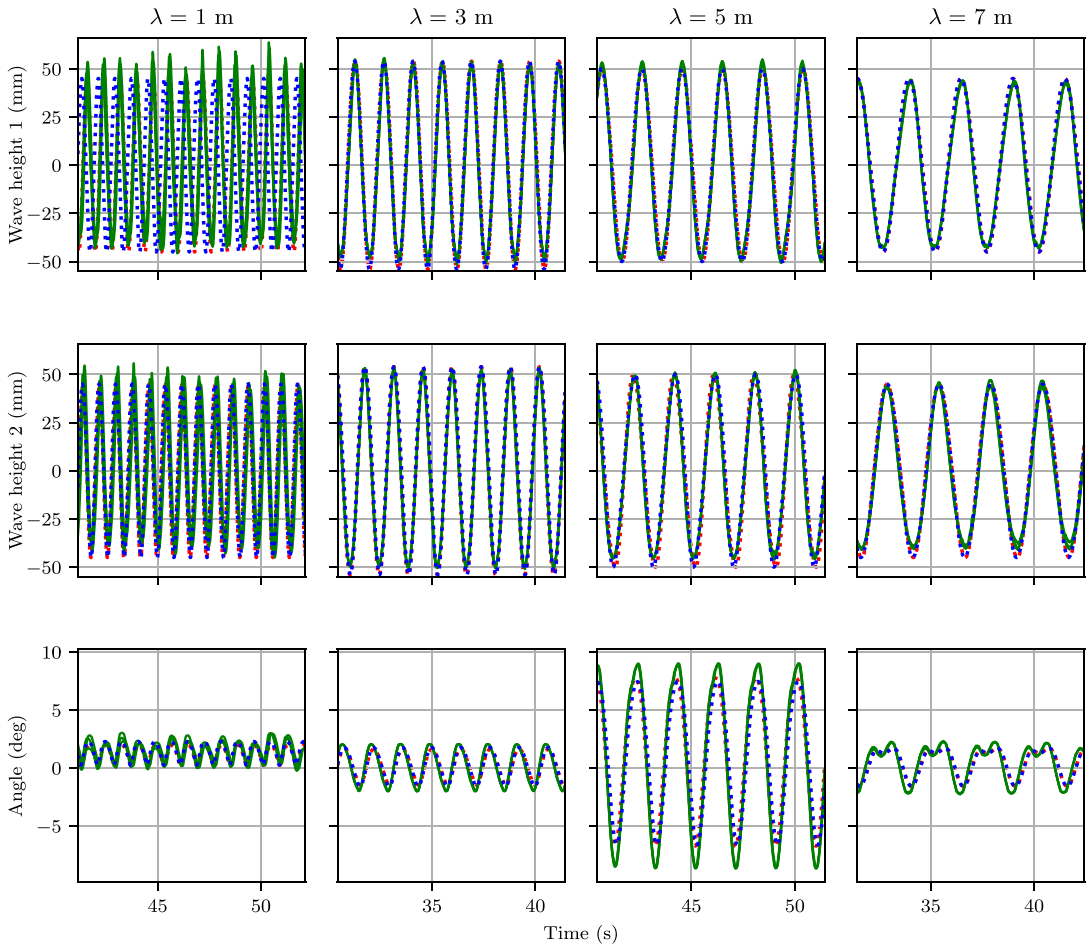

Fig. 4. Wave elevation for wave gauge 1 and 2 (top two rows) and pendulum response (bottom) in experiment and model. Wave height measured at pendulum rest location. Legend same as in Fig. 3, the additional red dotted line shows the results using the Rienecker–Fenton wave model (Rienecker and Fenton, 1981). (For interpretation of the references to colour in this figure legend, the reader is referred to the web version of this article.)

in determining *KC* is a modelling choice; we can equally well justify using the relative velocity of the pendulum with respect to the undisturbed wave particle velocity, as this is the velocity the tube truly experiences. That would make the procedure somewhat cumbersome, however. Second, we assume that the added mass and drag coefficients are equally valid for partially submerged cylinders as they are for the fully submerged cylinders from the original experiments.

4. Results and discussion

Here we describe the results of the experiment with the help of the analytical model. Then we compare the repetitions of the tests in order to investigate the variability of the surface elevation and the motion response of the pendulum. The waiting time of 15 min between each experiment was found to be sufficient because the wave gauge signal at the start of a new experiment was of the order of the calibration error of the wave gauges.

4.1. Comparison with analytical model

The comparison between experiments starts after the wave elevation at the second wave gauge (next to the pendulum) has reached the desired level. The 20 s of signal after that is input to our analysis. After that, there will be reflection from the longest wave components that exist due to ramping up the wave maker signal. The simulations are started at arbitrary time instances and run for 20 s. Then the transient response is cut off and the 'steady' part is compared to the previously selected 20 s of the experiment. Time synchronization between the experiments is done using a synchronization pulse. To synchronize the experiments with the numerical results the second wave gauge (WHM 2) and modelled surface elevation at the pendulum are matched.

Table 2
Ratio of modelled response due to a 10% lower and higher wave amplitude compared to the original wave amplitude.

η_a	$R\|\lambda = 1$ m	$R\|\lambda = 3$ m	$R\|\lambda = 5$ m	$R\|\lambda = 7$ m
+10%	1.24	1.17	1.08	1.35
−10%	1.28	1.20	1.13	1.40

The measured and modelled waves are plotted in Fig. 4: in green the three repetitions of the experiment and in blue dashed lines the analytical model. We aimed for 50 mm wave amplitude in all tests, which is close to what was achieved (an average of $\eta_a = 45, 54, 50, 45$ mm for $\lambda = 1, 3, 5, 7$ m respectively). The steepness of the waves equals $H/\lambda = 0.090, 0.036, 0.020, 0.013$, the steepest wave therefore is slightly over half of the breaking limit of 1/7. Wave breaking is not expected, but the shortest wave demonstrates nonlinear behaviour. As the wave length λ depends on wave height for steep waves we see a slight phase difference between simulations and experiment in WHM 1 for the shortest (and steepest) wave.

Fig. 4 shows that the free surface extremes are somewhat irregular. These irregularities do not repeat well between tests, as becomes apparent from the green lines for $\lambda = 1$ m that do not completely overlap. For the other wave lengths, the green lines overlap is nearly complete.

Additionally Fig. 4 shows the pendulum response for the four wave lengths: positive response means the pendulum swings towards the wave maker. Recall that the dry natural period of the pendulum was found to be 1.64 s. The wet natural period of the pendulum is expected to be higher because of added mass.

The first thing that stands out is the average value of the response, which is close to zero for all but the 1 m wave length. Apparently, loading the pendulum with a wave period much lower than the natural period results in a mean position shift. This mean position shift marks the nonlinearity in the response, as the incoming wave is nearly sinusoidal with zero mean. We also observe that the pronounced maxima, and the irregularity of the maxima that are present in the surface elevation, are transferred to the pendulum motion.

The response to the 5 m wave is highest, indicating that resonance occurs for a period close to this wave's period. As expected, the natural period for our wet-and-dry pendulum is higher because of added mass, which cannot be assumed constant because the pendulum transitions from dry to wet intermittently. A clear indication that the resonance period of the pendulum with added mass is between the periods for the waves with $\lambda = 3$ m and $\lambda = 5$ m, is that the phase between the wave height and the pendulum response changes from in-phase to counter-phase. Finally, we reflect on the shape of the 7 m wave signal. Here there are two maxima: the first one is from the free vibration stage, when the pendulum is dry. When it is swinging back, the pendulum is grazed by the wave, giving a second maximum. We can see energy is added in this latter peak because it is higher than the previous one. The wave period is long enough to allow the pendulum to go fully in the other direction and back, after which the process repeats. For even longer waves we expect this to be more pronounced (although this could not be tested due to stroke limitations of the wave maker). This is also a clear nonlinear effect. The incoming 7 m wave is close to sinusoidal as shown by the wave gauges. Then the double peak in the response demonstrates that higher frequency components were generated in the interaction between pendulum and waves.

In Fig. 4, and more clearly 5, the red dotted line shows the wave profile following Rienecker and Fenton (1981) and the response of the pendulum when using this wave model with the higher frequency components. The wave height at wave gauges 1 and 2 is very similar to that of the Airy model, even when zooming in. The pendulum response to the Rienecker–Fenton wave is somewhat lower than for the Airy wave, which is explained by the crests of the Rienecker–Fenton wave being sharper. With sharper crests the pendulum is under water for less time, allowing less time for energy transfer. As the waves become longer, meaning less steep, the wave becomes more sinusoidal and the models overlap again.

The wave height is not exactly constant during a single test, due to for instance start up effects or interaction with the pendulum. It is therefore interesting to investigate by means of the analytical model what the sensitivity of the response is to a change in the wave amplitude. Fig. 5 shows two additional lines compared to Fig. 4, representing the response to a regular wave with a 10% bigger or smaller amplitude. A 10% higher amplitude means 10% higher velocity, with quadratic drag that should lead to a 21% larger response. Table 2 shows what this 10% change in wave amplitude does. It gives the ratio R of increased or reduced pendulum amplitudes over the original response amplitude, for all wave lengths. Surprisingly, the 5 m wave which excites the pendulum near its natural frequency shows the least sensitivity to change in amplitude. The effect of increasing the amplitude is smaller than the effect of decreasing it. Another counter-intuitive finding is that the expected ratio of 1.21 is only found for the 3 m wave. For the other wave lengths, wetness clearly also has a large influence on the sensitivity of the response amplitude to changes in the wave amplitude.

The analytical model is a good representation of the experiment because it captures important aspects of the dynamic interaction between waves and pendulum and allows us to investigate the experimental results in more detail. From the comparison with the analytical model we find that the main drivers for nonlinear motion behaviour are the wetting and drying of the pendulum and the drag on the cylinder when it is under water. Note, however, in Fig. 5 that the response from the experiment is not inside the band formed by the analytical results with lower and higher amplitudes. This is an

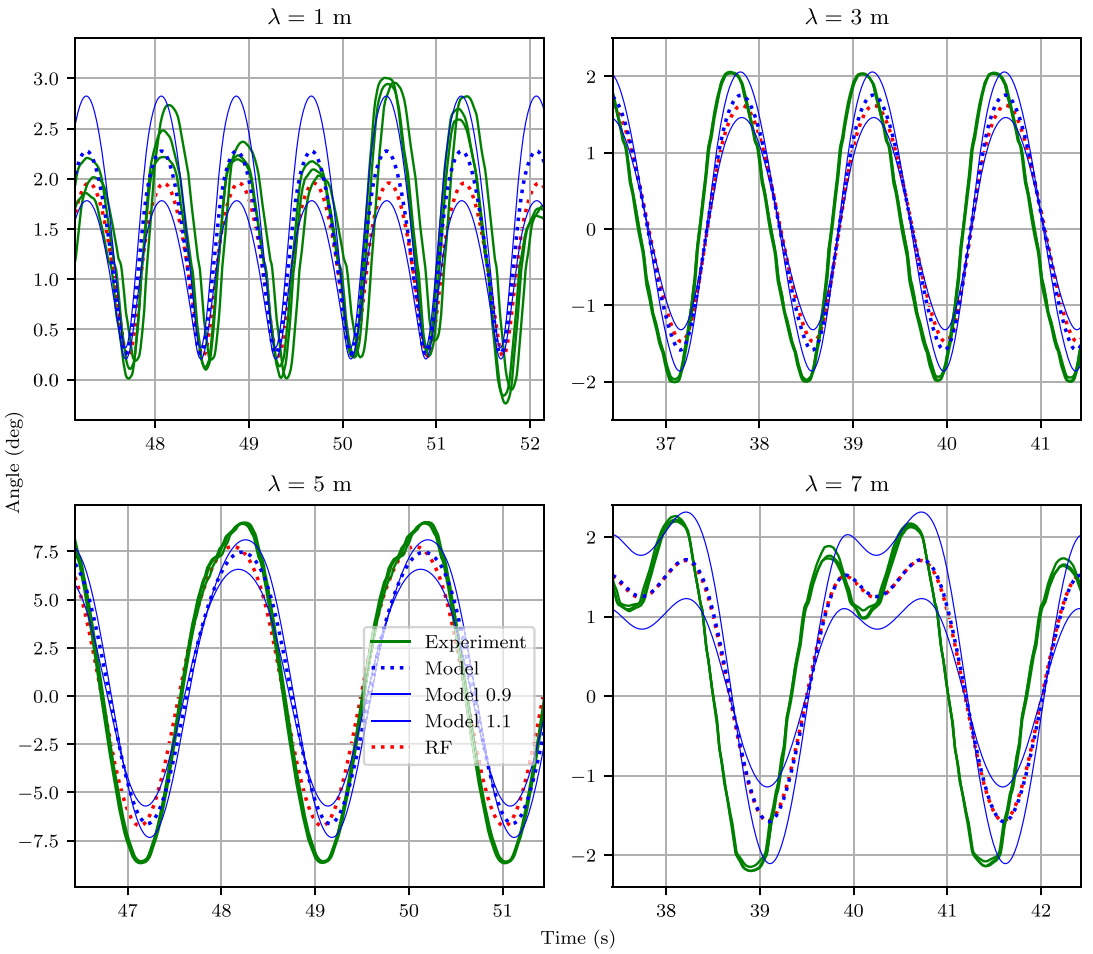

Fig. 5. Detailed response of the pendulum. The model response has a band representing the outcomes when the wave amplitude is increased or decreased by 10%. RF is the nonlinear wave model of Rienecker and Fenton (1981).

indication that in the experiment more is going on than can be captured by the analytical model. The water entry, buoyant behaviour and water exit are included in the experiment but not in the model. Structures in the interface between water and air are notoriously difficult to study by means of numerical models, because the intermittent presence of the structure breaks the continuity of the interface. Apparently, even for situations that are not that violent, modelling a structure that is in one medium for some time, and then transitions to the other medium for the next stretch of time, will require numerical techniques like Volume-of-Fluid or Level Set to capture the air–water interface near the structure. This is why we believe the experiment can be a useful benchmark for the community that works on developing these techniques.

4.2. Variability

In Fig. 5 the variability (dissimilarity or irregularity of surface and pendulum position from period to period) is largest for the steepest wave with $\lambda = 1$ m. The variability in the surface elevation is transferred to the angular position of the pendulum. But is the variability of the angular position as large as of the surface elevation?

Loading as a result of wave interaction with free-surface-piercing structures is highly variable (Bullock et al., 2007). It was reported that – locally – pressures on a wall resulting from the same (or highly similar) wave input were strongly dissimilar, but also that – globally – the wave force on the wall varied between experiments with the same input (Hofland et al., 2010). Among others, Bullock et al. (2007) and Hofland et al. (2010) also found that the impulse, which is the integral of force over a meaningful time span, between experiments shows less variability. The analyses using impulse have in common that the structures are fixed and rigid, and therefore cannot undergo a change of momentum. Translating this approach to our experiment with a structure that is free to move, leads to the hypothesis that the variability of the motion response is smaller than that of the wave input.

Figs. 6–9 show the variability of the measured surface elevation at WHM 2 and the measured angle of the pendulum. Here we divided the signal in parts as long as the period of the incoming wave. All these parts are then shifted to start

Table 3
Summary of the results: wave length, test series, number of tests n, mean and coefficient of variation of maxima response θ and wave height η.

λ, series	n	Mean max θ	Mean max η	CoV max θ	CoV max η
(1.0, 300)	28	2.36	47.8	0.230	0.100
(1.0, 304)	28	2.40	49.6	0.176	0.0874
(1.0, 308)	28	2.32	47.9	0.170	0.0759
(3.0, 301)	15	2.03	52.9	0.0551	0.0316
(3.0, 305)	15	2.02	52.9	0.0596	0.0305
(3.0, 309)	15	2.04	51.8	0.0561	0.0315
(5.0, 302)	10	9.00	49.6	0.0143	0.0323
(5.0, 306)	10	8.87	49.2	0.0217	0.0250
(5.0, 310)	10	8.92	48.4	0.0143	0.0195
(7.0, 303)	7	2.14	44.8	0.0254	0.0376
(7.0, 307)	7	2.15	43.6	0.0332	0.0181
(7.0, 311)	7	2.22	43.1	0.0324	0.0136

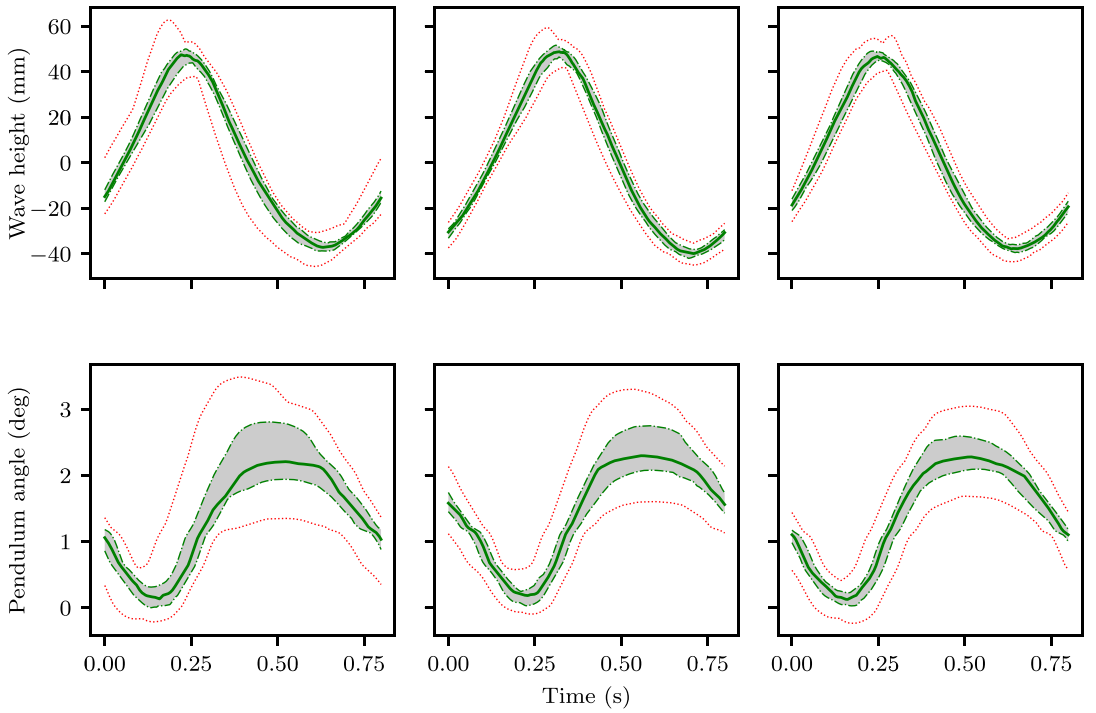

Fig. 6. Surface elevation (top) and response (bottom) in experiments for wave length $\lambda = 1$ m, with statistics over 28 periods. Left, middle and right column represent the first, second and third repetition of the test. Mean position at a time indicated by continuous green, 25th and 75th percentile indicated by dashed green and the grey band, minimum and maximum values indicated by dotted red. (For interpretation of the references to colour in this figure legend, the reader is referred to the web version of this article.)

at the same time. The minimum, maximum and, 25th, 50th and 75th percentile are calculated at every time instant and plotted in a single graph per experiment repetition. The top row shows the wave height at the pendulum, the bottom row shows the pendulum angle. Each column is one repetition of the experiment with the same input parameters. Table 3 shows a summary of the peaks of the wave elevation η and the pendulum response θ as well as the number of peaks n. For both of these variables the mean and coefficient of variation (CoV, standard deviation divided by mean) are given.

For the longer wave lengths $\lambda \geq 5$ m in Figs. 8 and 9 we see the 25th and 75th percentile results visually overlapping, meaning there is not much variability. This is also shown in Table 3. For $\lambda = 3$ m we see a surface elevation with hardly any variability, but a larger variability for the pendulum angle. The shortest wave $\lambda = 1$ m has the largest variability in both surface elevation and pendulum angle, which is true for all repetitions. For almost all experiments, the pendulum response has larger coefficient of variation than the wave height. This finding disproves the hypothesis, which stated that the variability of the fluid is local and would be smeared out in the global response of a structure. Instead variability of the fluid is amplified in the structural response. Note in Table 3 that the $\lambda = 1$ m wave of series 300 has a coefficient of variation of 0.10 on the wave elevation, giving a coefficient of variation of 0.23 for the maximum angle. A similar sensitivity was found with the analytical model for this wave length, as shown in Table 2.

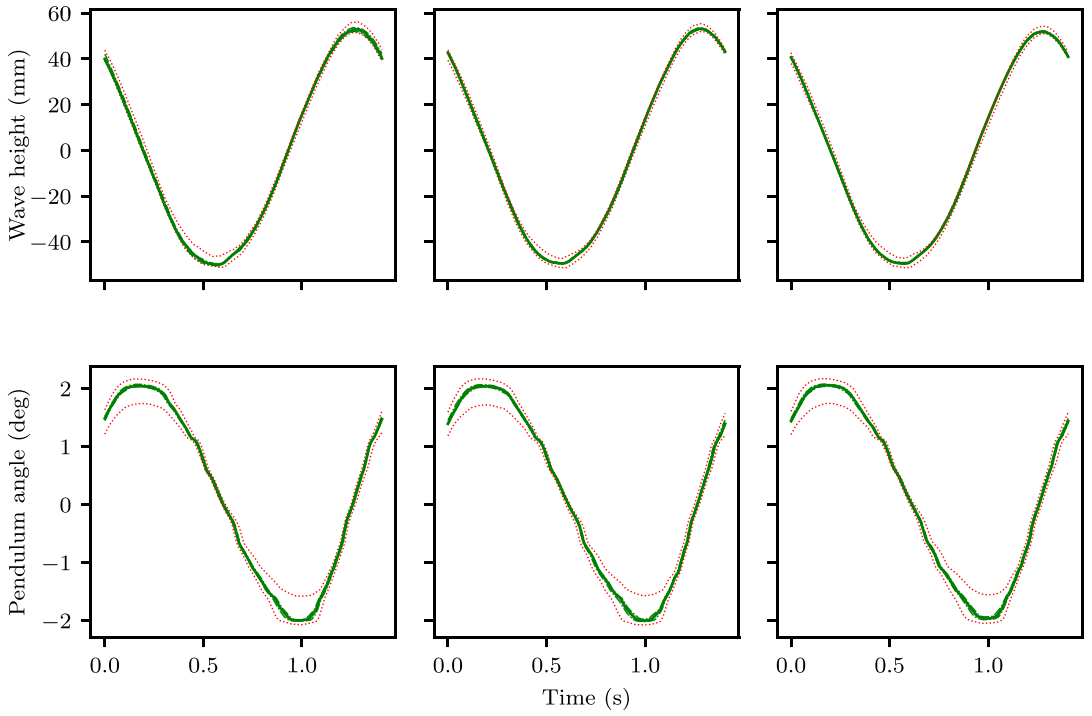

Fig. 7. Surface elevation (top) and response (bottom) in experiments for $\lambda = 3$ m, statistics over 15 periods. Description as in Fig. 6.

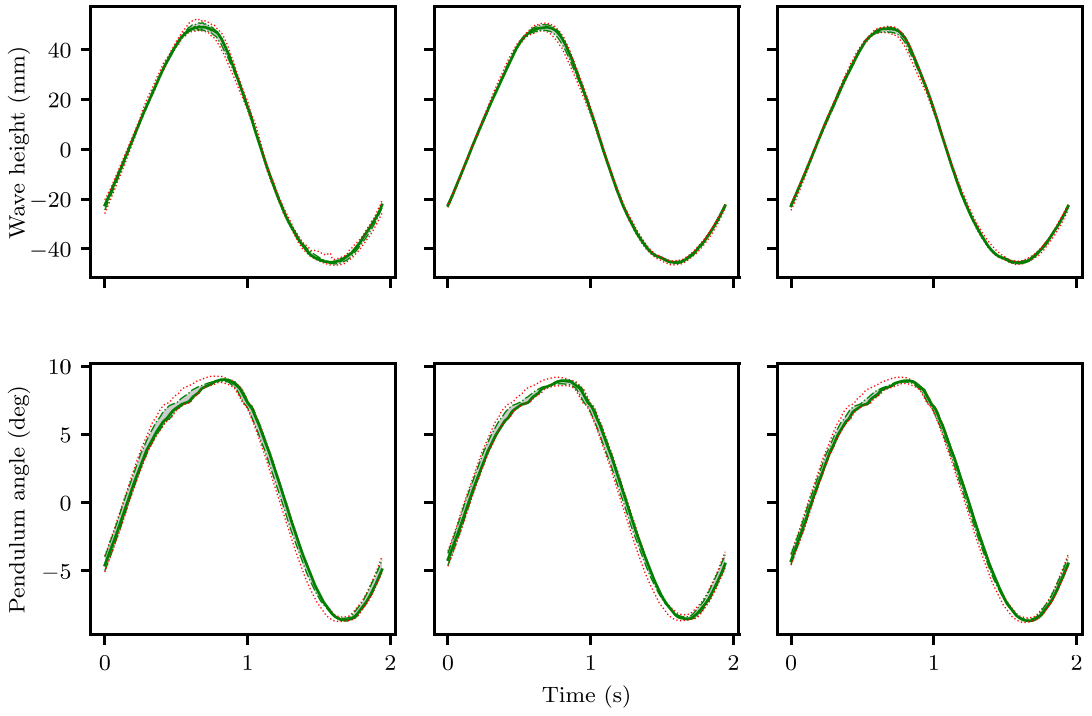

Fig. 8. Surface elevation (top) and response (bottom) in experiments for $\lambda = 5$ m, statistics over 10 periods. Description as in Fig. 6.

We conclude that the variability in the wave is amplified by the interaction with the pendulum. Using the findings from Table 2 confirms that a small variation in wave amplitude can indeed in most cases cause a superlinear increase in

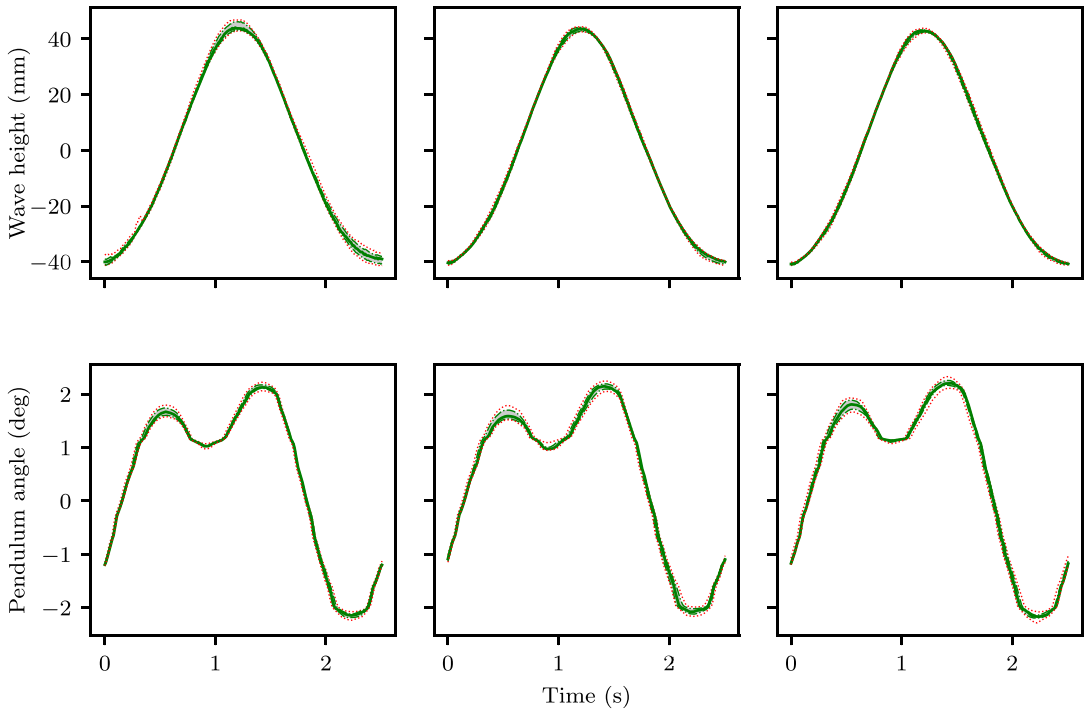

Fig. 9. Surface elevation (top) and response (bottom) in experiments for $\lambda = 7$ m, statistics over 7 periods. Description as in Fig. 6.

the response. Figs. 6–9 and Table 3 show that the pendulum response is more variable when the angle is positive, that is when the pendulum is dragged along by the wave. Underwater turbulence may explain the added uncertainty when the pendulum is loaded by the wave. The pendulum swings through the wake field it has left, which is different for every loading cycle. This would imply that the drag coefficient changes as the experiment progresses. Another possibility is that the structure starts moving already due to some droplet or filament. With this initial velocity the relative velocity between fluid and structure changes, giving a different response.

5. Conclusion

In this paper we have presented a benchmark experiment for fluid–structure interaction in maritime applications: a pendulum in monochromatic waves. The experiment captures water entry, submerged behaviour and water exit, modelling the large variations of wetted area that are typical for structures at sea. Large variations in wetted area cause different types of motion behaviour for different wave lengths. For a wave period much smaller than the dry natural period a mean position shift of the pendulum was observed. For a wave period much larger than the dry natural period, secondary local maxima in the signal of the pendulum position were observed. As expected, resonant motion behaviour for a wave period higher than the dry natural period was observed (higher because of added mass).

A reduced-order model was made which includes the added mass and drag components of the hydrodynamic loading, together with a wetness factor. A good comparison between model and experiment was obtained. The distinguishing dynamics of the wet-and-dry pendulum are captured by the model, and the Morison equations with the chosen coefficients are suitable for the entire wet-and-dry behaviour. The main drivers for nonlinearity are the wetting and drying and the drag. Seeing the small angles we obtained confirms buoyancy was rightfully disregarded from the model. There is no reason to assume that inclusion of air drag or buoyancy would have altered the results significantly.

A sensitivity analysis with the model that varied the wave amplitude demonstrated that model and experiment differ in details. A better correspondence would require a model that is able to represent the water entry and exit phenomena. Going into more detail it should model the wake of the pendulum as well as droplets and filaments. On the other hand, using linearized potential flow with small surface waves proved to be good enough.

The variability in surface elevation for waves with $\lambda \geq 3$ m was low, the variability of the shortest wave length was clearly the largest. For nearly all experiments the variability of the surface elevation was amplified in the response of the pendulum. This is confirmed by the sensitivity study, which showed that a 10% difference in wave amplitude gives a larger than 10% increase in pendulum response for all wave lengths except the 5 m wave. A hypothesis, extended from the literature about using impulse to interpret wave loading on non-moving structures, that the variability in the motion

of the structure should be lower than that of surface elevation, could not be confirmed. The variability was also found to be larger when the pendulum is dragged along by the wave, than when the pendulum moves back through air.

We believe that the presented experiment is a good benchmark for maritime FSI problems. The experiment could be augmented by investigating local vibrations of the structure, or additional (plastic) hinges. This will keep the experiment simple, but allows validation of other FSI phenomena. Another idea would be to repeat these tests for focused waves instead of monochromatic waves. Focused waves can be higher, and have a larger horizontal velocity when they break, increasing the water entry forces.

CRediT authorship contribution statement

R.W. Bos: Conceptualization, Methodology, Software, Validation, Formal analysis, Investigation, Data curation, Writing - original draft, Writing - review and editing, Visualization. **P.R. Wellens:** Conceptualization, Methodology, Software, Validation, Formal analysis, Investigation, Data curation, Writing original draft, Writing - review & editing, Supervision.

Declaration of competing interest

The authors declare that they have no known competing financial interests or personal relationships that could have appeared to influence the work reported in this paper.

Acknowledgements

We kindly thank the following students for their involvement in this project: Jochem Nonhebel, Bauke Vendeloo, Mike Blom, Sven Klinkhamer, Joris Vleer, Hoang Nguyen, David Pavilons, Bram Hoeksma and Floris van Ingen. We also thank the technical staff of the towing tank for their support: Jennifer Rodrigues Monteiro, Jasper den Ouden, Pascal Taudin Chabot, Peter Poot and Frits Sterk.

This work is part of the research programme 'SLING' with project number P14-10 which is (partly) financed by the Netherlands Organisation for Scientific Research (NWO).

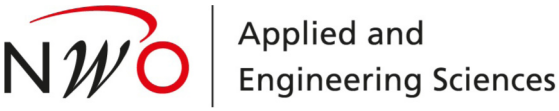

References

Andreeva, Tatiana, Alevras, Panagiotis, Naess, Arvid, Yurchenko, Daniil, 2016. Dynamics of a parametric rotating pendulum under a realistic wave profile. Int. J. Dyn. Control 4 (2), 233–238. http://dx.doi.org/10.1007/s40435-015-0168-z.

Bennett, S.S., Hudson, D.A., Temarel, P., 2013. The influence of forward speed on ship motions in abnormal waves : Experimental measurements and numerical predictions. J. Fluids Struct. 39, 154–172. http://dx.doi.org/10.1016/j.jfluidstructs.2013.01.006.

Botia-Vera, E., Souto-Iglesias, A., Bulian, G., Lobovsky, L., 2010. Three SPH novel benchmark test cases for free surface flows. In: 5th ERCOFTAC SPHERIC Workshop on SPH Applications. pp. 146–153.

Bullock, G.N., Obhrai, C., Peregrine, D.H., Bredmose, H., 2007. Violent breaking wave impacts. Part 1: Results from large-scale regular wave tests on vertical and sloping walls. Coast. Eng. 54 (8), 602–617. http://dx.doi.org/10.1016/j.coastaleng.2006.12.002.

Castellino, M., Sammarco, P., Romano, A., Martinelli, L., Ruol, P., Franco, L., De Girolamo, P., 2018. Large impulsive forces on recurved parapets under non-breaking waves. a numerical study. Coast. Eng. 136 (June), 1–15. http://dx.doi.org/10.1016/j.coastaleng.2018.01.012.

Dolfo, G., Castex, D., Vigué, J., 2016. Damping mechanisms of a pendulum. Eur. J. Phys. 37 (6), http://dx.doi.org/10.1088/0143-0807/37/6/065004.

Draycott, S., Payne, G., Steynor, J., Nambiar, A., Sellar, B., Venugopal, V., 2019. An experimental investigation into non-linear wave loading on horizontal axis tidal turbines. J. Fluids Struct. 84, 199–217. http://dx.doi.org/10.1016/j.jfluidstructs.2018.11.004.

Feng, Pei Yuan, Ma, Ning, Gu, Xie Chong, 2017. Long-term prediction of speed reduction due to waves and fuel consumption of a ship at actual seas. In: Proceedings of the ASME 2010 29th International Conference on Ocean, Offshore and Arctic Engineering. pp. 1–10.

Hayatdavoodi, Masoud, Ertekin, R. Cengiz, 2015. Wave forces on a submerged horizontal plate - Part I : Theory and modelling. J. Fluids Struct. 54, 566–579. http://dx.doi.org/10.1016/j.jfluidstructs.2014.12.010.

Hayatdavoodi, Masoud, Treichel, Kayley, Ertekin, R. Cengiz, 2019. Parametric study of nonlinear wave loads on submerged decks in shallow water. J. Fluids Struct. 86, 266–289. http://dx.doi.org/10.1016/j.jfluidstructs.2019.02.016.

Hofland, Bas, Kaminski, Miroslaw L., Wolters, Guido, 2010. Large scale wave impacts on a vertical wall. In: Proc. of the ICCE.

Kamra, Mohamed M., Salami, Jabir Al, Sueyoshi, Makoto, Hu, Changhong, 2019. Experimental study of the interaction of dambreak with a vertical cylinder. J. Fluids Struct. 86, 185–199. http://dx.doi.org/10.1016/j.jfluidstructs.2019.01.015.

Kaplan, P., Silbert, M.N., 1976. Impact forces on platform horizontal members in the splash zone. In: Proceedings of the Annual Offshore Technology Conference. pp. 749–758.

Kim, Mingyu, Hizir, Olgun, Turan, Osman, Day, Sandy, Incecik, Atilla, 2017. Estimation of added resistance and ship speed loss in a seaway. Ocean Eng. 141 (September), 465–476. http://dx.doi.org/10.1016/j.oceaneng.2017.06.051.

Lenci, S., Brocchini, M., Lorenzoni, C., 2012. Experimetnal rotations of a pendulum on water waves. J. Comput. Nonlinear Dyn. 7, http://dx.doi.org/10.1115/1.4004547.

Lenci, S., Rega, G., 2011. Experimental versus theoretical robustness of rotating solutions in a parametrically excited pendulum: A dynamical integrity perspective. Physica D 240, 814–824.

Liao, Kangping, Hu, Changhong, Sueyoshi, Makoto, 2015. Free surface flow impacting on an elastic structure: Experiment versus numerical simulation. Appl. Ocean Res. 50, 192–208. http://dx.doi.org/10.1016/j.apor.2015.02.002.

Losada, M.A., Merino, J., 1987. An energy approach to non-breaking wave- induced motion of bottom sediment particles. Coast. Eng. 11, 159–173.

Lugni, C., Bardazzi, A., Faltinsen, O.M., Graziani, G., 2014. Hydroelastic slamming response in the evolution of a flip-through event during shallow-liquid sloshing. Phys. Fluids 26, http://dx.doi.org/10.1063/1.4868878.

Mathai, V., Govardhan, R.N., Arakeri, V.H., 2015. On the impact of a concave nosed axisymmetric body on a free surface. Appl. Phys. Lett. 106 (6), http://dx.doi.org/10.1063/1.4907555.

Mathai, V., Loeffen, L.A.W.M., Chan, T.T.K., Wildeman, S., 2019. Dynamics of heavy and buoyant underwater pendulums. J. Fluid Mech. 862, 348–363. http://dx.doi.org/10.1017/jfm.2018.867.

Mei, X., Liu, Y., Yue, D.K.P., 1999. On the water impact of general two-dimensional sections. Appl. Ocean Res. 21 (1), 1–15. http://dx.doi.org/10.1016/S0141-1187(98)00034-0.

Morison, J.R., Johnson, J.W., Schaaf, S.A., 1950. The force exerted by surface waves on piles. J. Pet. Technol. 2, http://dx.doi.org/10.2118/950149-G.

Porter, R., 2019. The coupling between ocean waves and rectangular ice sheets. J. Fluids Struct. 84, 171–181. http://dx.doi.org/10.1016/j.jfluidstructs.2018.09.004.

Rienecker, M.M., Fenton, J.D., 1981. A fourier approximation method for steady water waves. J. Fluid Mech. 104, 119–137.

Sader, John E., Cosse, Julia, Kim, Daegyoum, Fan, Boyu, Gharib, Morteza, 2016. Large-amplitude flapping of an inverted flag in a uniform steady flow - a vortex-induced vibration. J. Fluid Mech. 793, 524–555.

Sarpkaya, Turgut, 1986. Force on a circular cylinder in viscous oscillatory flow at low Keulegan–Carpenter numbers. J. Fluid Mech. 165, 61–71. http://dx.doi.org/10.1017/S0022112086002999.

Van Nuffel, D., Vepa, K.S., De Baere, I., Lava, P., Kersemans, M., Degrieck, J., De Rouck, J., Van Paepegem, W., 2014. A comparison between the experimental and theoretical impact pressures acting on a horizontal quasi-rigid cylinder during vertical water entry. Ocean Eng. 77, 42–54. http://dx.doi.org/10.1016/j.oceaneng.2013.11.019.

Wagner, H., 1932. Über sto- und gleitvorgänge an der oberfläche von flüssigkeiten. Z. Angew. Math. Mech. 12.

Weidenfeld, Michael, Arad, Eran, 2018. Mitigating the sound of a flapping airfoil using optimal structural properties distributions. J. Sound Vib. 432, 235–248.

Wellens, Peter R., Bos, Reinier W., 2020. Experimental data for a wet-and-dry pendulum suspended in monochromatic waves. Delft University of Technology; 4TU.ResearchData, http://dx.doi.org/10.4121/13187594.

Young, Y.L., Wright, T., Yoon, H., Harwood, C.M., 2020. Dynamic hydroelastic response of a surface-piercing strut in waves and ventilated flows. J. Fluids Struct. 94, 102899. http://dx.doi.org/10.1016/j.jfluidstructs.2020.102899.

Zheng, Siming, Zhang, Yongliang, 2017. Analysis for wave power capture capacity of two interconnected floats in regular waves. J. Fluids Struct. 75, 158–173. http://dx.doi.org/10.1016/j.jfluidstructs.2017.08.010, http://dx.doi.org/10.1016/j.jfluidstructs.2017.08.010.